dσ) → dσ* state, which is a combination of $4A_{2u}$ and $8A_{2u}$ of singlet origin. The Xσ donor orbitals are less stable than for H_2O, so that a lower energy axial LMCT is reasonable. The similarity in energy for the intense band for the diammine and dihydroxo complexes suggests that the axial ligands have σ orbitals of nearly the same stability in the two cases.

The lower energy bands for these complexes are not very well resolved and consist of shoulder absorption between 2.3 and 3.2 μm^{-1}. In both cases, the MCD has the appearance of a negative *A* term (for band I for the diammine complex and for band II for the dihydroxo complex). This MCD *A* term is ascribed to the transition to $4E_u$ ($2e_g \rightarrow b_{2u}$, $d\pi^* \rightarrow \sigma^*PtO_4$), which is expected to be the lowest energy negative *A* term of singlet parentage. This is the same state suggested at low energy in the dihalo complexes (and possibly also present among the low-energy bands for the diaqua complex). For the dihydroxo complex, an additional negative MCD feature is observed at 3.31 μm^{-1}, but no corresponding absorption is resolved. This MCD minimum signals the presence of another state between those associated with bands II and III. It is likely due to a transition to a state of spin-forbidden origin such as $8E_u$, but little more can be concluded from the present results. Finally, the weak band I for the dihydroxo complex is assigned as transitions to states of spin-forbidden origin $3B_u$ and $2A_{2u}$, which are expected to be at low energy.

Concluding Remarks. The energy level scheme in Figure 5 provides a basis for visualizing the excited configurations and states of Table II, which in turn provide a satisfactory interpretation of the spectra for the binuclear sulfato and hydrogen phosphatodiplatinum(III) complexes. Of course, other interpretations may be possible, but the assignments proposed here are internally consistent in energy, intensity, and MCD *A* term sign. One of the most important results to come from this study is the observation of *A* terms for the intense high-energy bands for the diaqua and dihalo complexes. These *A* terms demonstrate the presence of E_u states of LMCT origin rather than the A_{2u} (Xσ,dσ)dσ* states assumed earlier.[7,12] Furthermore, a consideration of *A* term signs allows more detailed assignments of these intense bands. The diaqua complexes reveal LMCT involving the bridge oxygen ligands while the dihalo complexes give rise to LMCT involving the axial halide ligands. The negative *A* terms observed for both the intense bands for the diaqua complexes and the weaker lower energy bands for the diammine and dihydroxo complexes point out the spectroscopic accessibility of the σ*PtO$_4$ orbitals b_{1g} and b_{2u}. The (Xσ, dσ) → dσ* excitation for the diaqua and dihalo complexes is undoubtedly at higher energy than the present measurements allow, whereas the diammine and dihydroxo complexes with stronger axial donor ligands have transitions to (Xσ,dσ)dσ* excited states at lower energy.

Note Added in Proof. A study of the $Pt_2(SO_4)_4X_2^{n-}$, X = H_2O, Cl⁻, and Br⁻, ions was reported after our paper was submitted.[22] Transition assignments for the intense high-energy bands exhibited by these ions are presented which closely parallel those advanced earlier for the HPO$_4^{2-}$ complexes[12] and involve promotion to dσ*. These assignments should be reconsidered in light of the present MCD *A*-term results for these high-energy bands.

(22) Newman, R. A.; Martin, D. S.; Dallinger, R. F.; Woodruff, W. H.; Stiegman, A. E.; Che, C.-M.; Schaefer, W. P.; Miskowski, V. M.; Gray, H. B. *Inorg. Chem.* **1991,** *30,* 4647.

Contribution from Fuel Science Department 6211, Sandia National Laboratories, Albuquerque, New Mexico 87185, Department of Chemistry, University of New Mexico, Albuquerque, New Mexico 87131, and Department of Chemistry and Biochemistry, University of Notre Dame, Notre Dame, Indiana 46556

Effects of π–π Interactions on Molecular Structure and Resonance Raman Spectra of Crystalline Copper(II) Octaethylporphyrin

L. D. Sparks,[†] W. Robert Scheidt,*,[‡] and J. A. Shelnutt*,[†]

Single-crystal resonance Raman measurements were performed on two crystalline phases of copper(II) octaethylporphyrin (CuOEP): triclinic A and triclinic B forms. These are compared to previously acquired resonance Raman data on the triclinic A and triclinic B phases of nickel(II) octaethylporphyrin (NiOEP). The difference in crystal packing between the triclinic A and B structures allows for more extensive π–π interactions in the B form than in the A form. Differences in the single-crystal Raman spectra of the triclinic A and B forms of both Cu- and NiOEP are attributed to these π–π interactions. Specifically, the Raman core-size marker lines, ν_3, ν_2, and ν_{10}, and the oxidation-state marker line, ν_4, are affected by the different packing interactions in the two crystals, and the same Raman shifting patterns between the triclinic A and B phases are observed for both Cu- and NiOEP. The metal centers exert a slight influence over the packing-induced frequency shifts in the Raman modes. Spectral results on the CuOEP crystals are also compared to solution Raman data on π–π aggregated and monomeric copper(II) uroporphyrin (CuUroP). Similar to the A and B forms of NiOEP, the CuOEP triclinic A and B crystalline phases mimic the monomer and salt-induced aggregate of CuUroP in solution, as evidenced by similar magnitude upshifts in the Raman modes upon aggregation. A comparison of the structure calculated using molecular mechanics and the structure obtained from X-ray diffraction gives some insight into the effect that π–π interactions have on the structure of CuOEP in the triclinic B crystal.

Introduction

The effects of π–π interactions on the molecular structure and the chemical and photophysical properties of metalloporphyrins are not well understood. Stacking interactions with aromatic amino acid residues could play a role in porphyrin binding to proteins and in modulation of the chemistry and photophysics of the porphyrin cofactors. Modulation of electron-transfer rates of photosynthetic pigments and modulation of chemical properties of heme proteins are two examples. Unfortunately, few experimental methods allow definitive investigation of π–π interactions between stacked porphyrin molecules or stacking interactions with aromatic residues. We are developing resonance Raman spectroscopy as a tool for the investigation and interpretation of the effects of π–π interactions in stacked systems.

Previously, the crystalline forms of nickel(II) octaethylporphyrin (NiOEP) were studied by resonance Raman spectroscopy for this purpose. The three crystalline phases of NiOEP (triclinic A and B and tetragonal) were investigated,[1] and the differences in Raman spectra between the triclinic A and B phases were interpreted in

---

terms of the $\pi-\pi$ interactions found in the triclinic B phase. The triclinic B form of NiOEP was found[1] to have a solid-state environment that is distinct from that reported[2] for the triclinic A and tetragonal phases. Specifically, this form has an extended $\pi-\pi$ stacking of individual NiOEP molecules and a small lateral shift compared to the triclinic A form. Therefore, comparison of the two solid-state NiOEP triclinic forms is somewhat like comparing monomeric and aggregated forms in solution, where the triclinic B phase models the $\pi-\pi$ solution aggregate and the triclinic A phase simulates the solution monomer. Solution spectra of the $\pi-\pi$ aggregate and monomeric forms of a nickel porphyrin in aqueous alkaline solution were obtained using nickel(II) uroporphyrin I (NiUroP), which aggregates upon addition of salt. Monomer–aggregate shifts in the structure-sensitive Raman lines were similar for the crystalline and solution experiments; that is, shifts were in the same direction and of similar magnitudes in the NiOEP crystals as in the NiUroP solutions.

In the present work, we have used resonance Raman spectroscopy to investigate two crystalline forms of copper(II) octaethylporphyrin (CuOEP), namely triclinic A and triclinic B. Pak and Scheidt[3] recently reported that the CuOEP triclinic B crystalline phase is isomorphous with the triclinic B phase of NiOEP in that the molecules of CuOEP also pack with an extended $\pi-\pi$ interaction along the c axis and exhibit a small lateral shift. To date, there have been no reports on the crystal structure of the CuOEP triclinic A phase, although the cell constants are known.[4] In this work, we compare the Raman spectra of single crystals of the two CuOEP phases, and we relate these to the previously reported Raman spectra of the triclinic A and B forms of NiOEP.[1] The single-crystal Raman results for the CuOEP triclinic A and B forms are also compared with those for the solution copper(II) uroporphyrin I (CuUroP) monomer and salt-induced dimer, respectively. Stackings in the crystalline forms of triclinic B CuOEP and NiOEP produce similar effects on the Raman spectra of these macrocycles. We also find similarities between the monomer–dimer spectral differences in solution and in the crystals. For example, the increase in frequency of the core-size marker lines[5,6] for aggregates in both the crystal and the solution (relative to the "monomer" forms) predicts a contraction of the central core.

Molecular mechanics (energy optimization) calculations were carried out on CuOEP with the triclinic A and B and tetragonal ethyl orientations observed for NiOEP. Comparison of structural data originating from the molecular mechanics calculations and from X-ray crystallographic studies demonstrates the effect on the structure of the porphyrin resulting from the presence or absence of $\pi-\pi$ interactions.

Materials and Methods

CuOEP Crystallization. CuOEP was prepared by insertion into H_2OEP in DMF solution.[7] Crystals of CuOEP (type B) were obtained by layering hexane over a methylene chloride solution and allowing the hexane to diffuse into the solution. Crystals of type A were obtained by slow evaporation of a methylene chloride solution of CuOEP to which H_2OEP had been added (sufficient to make the solution ~6% in H_2OEP).

Spectroscopic Studies. All Raman spectra were obtained using a dual-channel Raman spectrometer described previously.[8] For single-crystal Raman spectra, the spectrometer was used in the conventional single-channel mode; therefore, for accurate determination of Raman mode frequencies, several spectra of each crystalline form were recorded
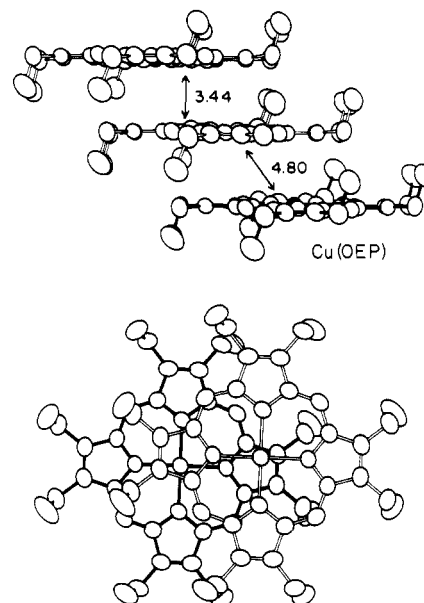

Figure 1. (a) Top: Edge-on view of the CuOEP $\pi-\pi$ aggregate in the triclinic B phase. Distances shown are the Cu–Cu separation and the mean plane separation. (b) Bottom: Overlap diagram showing two of the interacting CuOEP units displayed in Figure 1a.

and the average peak positions calculated from four separate spectra of each crystal. Peak positions for the Raman lines were determined from the fast-Fourier-transform (FFT) smoothed spectra, and average frequency differences and probable errors were determined. Less than 10 mW of the 457.9-nm radiation from an argon ion laser (Coherent) impinging at grazing incidence on a single crystal of CuOEP was used. Much of the incident light was reflected from the shiny facet of the crystal (especially in the case of triclinic A CuOEP) so that the absorbed light was less than or equal to 1 mW. At much higher powers, the crystal could be sublimed as a vapor. No sample heating was evident at the lower powers. Each of the Raman spectra consists of about 15 20-min scans of a 400-cm⁻¹ region of the spectrum. Spectral resolution was 4 cm⁻¹. No change in the CuOEP spectrum was noted during signal averaging, and no change was observed in the surface of the crystal when examined under a microscope at the end of data collection.

For solution samples, the metal uroporphyrin, Cu- or NiUroP (~5 × 10⁻⁵ M), in 0.1 M potassium hydroxide was added to one side of a partitioned cell and the dimer was added to the other side of the cell. The dimer was formed by saturating the Cu- or NiUroP solution with sodium chloride (~5.5 M). Laser excitation at 413.1 nm from a krypton ion laser was used for the solution samples, and scattered light was collected at 90° to the direction of propagation and polarization of the exciting laser light. Rotation of the sample cell at 50 Hz enables the two samples to be probed alternately by the laser radiation and prevents sample heating. Simultaneous collection of the spectra of the two samples allows for elimination of errors resulting from variations in instrument response and grating positioning. The two Raman spectra were subsequently modeled[9] using Lorentzian line shapes to fit the peaks. The sloped, linear baseline was allowed to vary, and a least-squares fit determined the position and line width of the peaks present in the spectra.

Molecular Mechanics Calculations. The Cu- and NiOEP molecules were constructed with the triclinic B, triclinic A, and tetragonal ethyl orientations. They were then energy-optimized using BIOGRAF software (Molecular Simulations, Inc.) which utilizes a conjugate-gradient minimization technique with a force field that we defined[10] on the basis of a normal-coordinate analysis of NiOEP[11] and the DRIEDING force field.[12] This force field was then modified slightly, on the basis of information contained in the X-ray crystal data for a series of first-row

(1) Brennan, T. D.; Scheidt, W. R.; Shelnutt, J. A. *J. Am. Chem. Soc.* **1988**, *110*, 3919.
(2) Cullen, D. L.; Meyer, E. F., Jr. *J. Am. Chem. Soc.* **1974**, *96*, 2095.
(3) Pak, R.; Scheidt, W. R. *Acta Crystallogr.* **1991**, *C47*, 431–433.
(4) Scheidt, W. R.; Ivanca, M. A. Unpublished results. Cell constants for the triclinic A form: a = 9.877 Å, b = 10.730 Å, c = 7.554 Å, α = 97.24°, β = 108.24°, γ = 92.69°.
(5) Spaulding, L. D.; Chang, C. C.; Yu, N.-T.; Felton, R. H. *J. Am. Chem. Soc.* **1975**, *97*, 2517.
(6) Spiro, T. G. In *Iron Porphyrins*; Lever, A. B. P., Gray, H. B., Eds.; Addison-Wesley: Reading, MA, 1982; Part II, Chapter 3.
(7) Adler, A. D.; Longo, F. R.; Kampas, F.; Kim, J. *J. Inorg. Nucl. Chem.* **1970**, *32*, 2443.
(8) Shelnutt, J. A. *J. Phys. Chem.* **1983**, *87*, 605.

(9) Stump, R. F.; Deanin, G. G.; Oliver, J. M.; Shelnutt, J. A. *Biophys. J.* **1987**, *51*, 605.
(10) Shelnutt, J. A.; Medforth, C. J.; Berber, M. D.; Barkigia, K. M.; Smith, K. M. *J. Am. Chem. Soc.* **1991**, *113*, 4077.
(11) (a) Abe, M.; Kitagawa, T.; Kyogoku, Y. *J. Chem. Phys.* **1978**, *69*, 4526. (b) Kitagawa, T.; Abe, M.; Ogoshi, H. *J. Chem. Phys.* **1978**, *69*, 4516. (c) Li, X.-Y.; Czernuszewicz, R. S.; Kincaid, J. R.; Spiro, T. G. *J. Am. Chem. Soc.* **1989**, *111*, 7012. (d) Li, X.-Y.; Czernuszewicz, R. S.; Kincaid, J. R.; Stein, P.; Spiro, T. G. *J. Phys. Chem.* **1990**, *94*, 47.
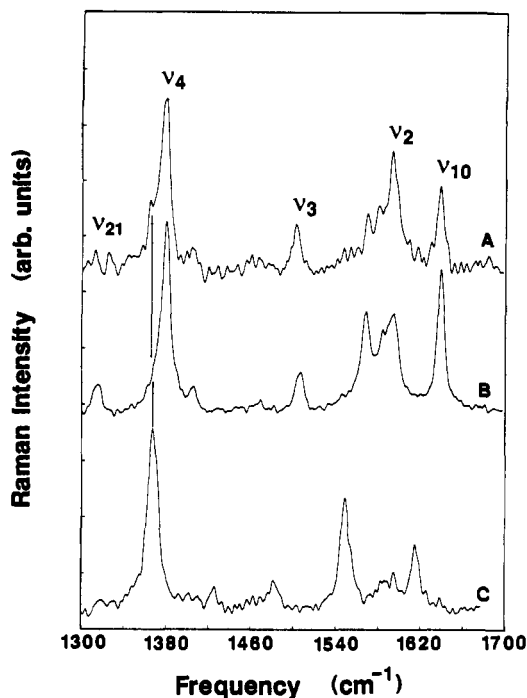(12) Mayo, S. L.; Olafson, B. D.; Goddard, W. A., III. *J. Phys. Chem.* **1990**, *94*, 8897.

Figure 2. Single-crystal Raman spectra for (A) triclinic A CuOEP, (B) triclinic B CuOEP, and (C) H_2OEP in the 1300–1700-cm^{-1} region.

transition metal porphyrins and published metal–metal bond distances.[13,14] Details of these calculations are given elsewhere.[10,13] The calculations were carried out and displayed on a 4D210 Power Series workstation (Silicon Graphics, Inc.).

Results

The structure of the CuOEP triclinic B crystal was reported previously.[3] Figure 1a shows the CuOEP triclinic B crystal packing and gives the Cu–Cu distance and the mean plane separation. Figure 1b shows the overlap in the aggregate stack. Only the cell parameters are known[4] for triclinic A CuOEP.

Figure 2 shows typical resonance Raman spectra of the two CuOEP crystalline forms and, for comparison, the spectrum of a form of free-base octaethylporphyrin (H_2OEP) that is isomorphous with the triclinic A form of CuOEP (H_2OEP is also isomorphous with the triclinic A phase of NiOEP). Formation of the CuOEP triclinic A phase apparently is dependent upon the presence of a small amount of H_2OEP in the crystallizing solution.[1] The Raman lines of the H_2OEP impurity are therefore expected to be more abundant in the CuOEP triclinic A crystal spectra shown in Figure 2. Indeed, the mode at 1366 cm^{-1} in the CuOEP triclinic A spectrum is due to the presence of H_2OEP.

Excitation at 457.9 nm is expected to enhance the Raman lines of CuOEP (Soret band at 410 nm in CS_2) more so than those of H_2OEP (Soret band at 383 nm).[15] This wavelength is not directly in resonance with either porphyrin Soret absorption maximum. However, excitation near the Soret band enhances totally symmetric modes of the porphyrin macrocycle and the spectra are dominated by Raman lines with frequencies >1000 cm^{-1}, corresponding to porphyrin π-bond stretching vibrations. For example, the totally symmetric modes ν_4, ν_3, and ν_2 are representative of the porphyrin C_α–N, C_α–C_m, and C_β–C_β bond stretches,[11] respectively.

Table I lists the frequencies of the major CuOEP Raman lines. The assignments given are based on those for NiOEP.[11] The Raman frequencies are the resultant averages of all the spectra

Table I. Frequencies (cm^{-1}) of Structure-Sensitive Raman Marker Lines of Cu- and NiOEP Crystals and Differences (Δ) between the Two Triclinic Forms and between the Dimer and Monomer Cu- and NiUroP

mode[a]	CuOEP freq		$\Delta(B-A)^d$		$\Delta(Ag-M)^d$	
	tri A	tri B	CuOEP	NiOEP[b]	CuUroP[c]	NiUroP[c]
ν_{21}	1313.9	1314.9	1.0 ± 0.8	1.2 ± 0.9	−0.4 ± 1.0	1.7 ± 1.0
ν_4	1379.7	1380.7	1.0 ± 0.2	2.5 ± 1.9	1.3 ± 0.1	1.4 ± 0.1
ν_3	1503.7	1507.6	3.9 ± 0.4	4.3 ± 1.6	2.6 ± 0.1	2.7 ± 0.2
ν_2	1593.4	1595.9	2.6 ± 0.8	2.9 ± 2.1	0.7 ± 0.1	2.9 ± 0.6
ν_{10}	1638.5	1640.9	2.4 ± 0.6	3.2 ± 2.4	2.7 ± 0.1	1.0 ± 0.3

[a] Assignments are taken from ref 11. [b] From ref 1. [c] This work. In NiUroP, only the planar form was used for ν_3 and ν_{10}, but a mixture of ruffled and planar forms was used for ν_{21}, ν_4, and ν_2. [d] Shifts were obtained from curve fits of Raman data. Ag = aggregate; M = monomer.

Table II. Calculated Minimum Energies (kcal/mol) without (and *with*) Partial Atomic Charges for CuOEP and NiOEP with the Ethyl Orientations of the NiOEP Crystalline Forms

	CuOEP			NiOEP		
	tri B	tri A	tet	tri B	tri A	tet
total	113.5	115.3	115.4	120.8	122.6	122.7
	146.0	*147.7*	*149.1*	*153.1*	*156.2*	*156.1*
bonds	7.1	7.6	7.6	10.3	10.8	10.7
	9.0	*9.0*	*9.5*	*12.2*	*11.7*	*12.5*
angles	77.7	78.4	78.4	77.8	78.5	78.5
	78.4	*78.8*	*79.0*	*78.5*	*79.1*	*79.2*
torsions	0.4	0.3	0.3	0.4	0.3	0.4
	0.9	*1.4*	*1.3*	*1.0*	*1.4*	*1.6*
inversions	0.0	0.0	0.0	0.0	0.0	0.0
	0.0	*0.0*	*0.0*	*0.0*	*0.0*	*0.0*
van der Waals	28.2	29.0	29.1	32.3	33.1	33.1
	27.3	*28.2*	*27.2*	*31.2*	*32.4*	*31.0*
electrostatic	0.0	0.0	0.0	0.0	0.0	0.0
	30.4	*30.3*	*32.1*	*30.3*	*31.6*	*31.7*

obtained of each crystalline form. $\Delta(B-A)$ signifies the difference between the average frequencies of triclinic A and B CuOEP. In the comparison of the triclinic A and B forms of CuOEP, small but significant differences in the frequency of the core-size marker lines,[5,6] ν_3, ν_2, and ν_{10}, are noted. These lines are higher by 2.4–3.9 cm^{-1} for the triclinic B form. The core-size marker lines are also sensitive to π-charge density in the macrocycle and oxidation state.[6,16–18] Significantly, the oxidation-state marker line, ν_4, increases by 1.0 cm^{-1} for the CuOEP triclinic B crystal. A shift of 1.0 cm^{-1} to higher frequency for the triclinic B form is also observed for ν_{21}. Previously recorded differences between the NiOEP triclinic A and B phases are listed in Table I for reference.[1] The direction of the shift, $\Delta(B-A)$, is the same for both CuOEP and NiOEP. The magnitude of the shifts for CuOEP is consistently less than that for NiOEP, but the individual differences are not statistically significant.

Table I also gives the Raman frequency differences between the monomeric and aggregated CuUroP and NiUroP solution species. The CuUroP data are consistent with previous results[19] for ν_3, ν_2, and ν_{10}. The NiUroP data are also consistent with previous results[20] for ν_4, ν_2, and ν_{10}, but the current data set gives a better signal-to-noise ratio and lower errors for the differences. Some errors in the NiUroP solution spectra can be attributed to other, interfering Raman lines. For example, ν_{19} appears at nearly the same frequency as does ν_2 but cannot be differentiated by the curve-fit program.[9] Also, since both ruffled and planar forms coexist in NiUroP solution, there is some interference from the ruffled forms. The NiUroP data were analyzed by curve fitting to resolve planar and ruffled conformers as described by Alden et al.[20]

(13) Sparks, L. D.; Medforth, C. M.; Park, M.-S.; Chamberlain, J. R.; Ondrias, M. R.; Senge, M. O.; Smith, K. M.; Shelnutt, J. A. Submitted for publication.

(14) *International Tables for X-ray Crystallography*; Kynoch Press: Birmingham, England, 1962; Vol. III (present distributor: Kluwer Academic Publishers, Dordrecht, The Netherlands).

(15) Gouterman, M. In *The Porphyrins*; Dolphin, D., Ed.; Academic: New York, 1978; Chapter 1.

(16) Yamamoto, T.; Palmer, G.; Salmeen, I. T.; Rimai, L. *J. Biol. Chem.* **1973**, *248*, 5211.

(17) Spiro, T. G.; Strekas, T. C. *J. Am. Chem. Soc.* **1974**, *96*, 338.

(18) Spiro, T. G.; Burke, J. M. *J. Am. Chem. Soc.* **1976**, *98*, 5482.

(19) Shelnutt, J. A.; Dobry, M. M.; Satterlee, J. D. *J. Phys. Chem.* **1984**, *88*, 4980.

(20) Alden, R. G.; Ondrias, M. R.; Shelnutt, J. A. *J. Am. Chem. Soc.* **1990**, *112*, 691.

Table III. Comparison of Selected Structural Parameters from the X-ray Crystal Structures (Italic) and Values Calculated Using the Ethyl Orientations of the Corresponding Crystal

	CuOEP crystals			NiOEP crystals		
	tri B[a]	tri A	tet	tri B[b]	tri A[c]	tet[c]
Bonds, Å						
M–N	1.999[d]	1.998[f]	1.998[f]	1.954[d]	1.956[f]	1.953[f]
	1.996			*1.946*	*1.958*	*1.929*
M–N	1.996[e]			1.951[e]		
	1.999			*1.958*		
N–C$_\alpha$	1.38	1.38	1.38	1.38	1.38	1.38
	1.38			*1.39*	*1.38*	*1.39*
C$_\alpha$–C$_m$	1.37	1.37	1.37	1.37	1.37	1.37
	1.37			*1.36*	*1.37*	*1.37*
C$_\alpha$–C$_\beta$	1.45	1.45	1.45	1.45	1.45	1.45
	1.45			*1.44*	*1.44*	*1.45*
C$_\beta$–C$_\beta$	1.35	1.35	1.35	1.35	1.35	1.35
	1.35			*1.33*	*1.35*	*1.36*
Angles, deg						
N–M–N	180.0	180.0	179.3	180.0	180.0	179.1
	180.0			*180.0*	*180.0*	*179.7*
C$_\alpha$–N–C$_\alpha$	106.1	106.0	106.0	104.5	104.5	104.5
	105.5			*104.3*	*103.9*	*105.1*
C$_\alpha$–C$_m$–C$_\alpha$	125.1	125.2	125.2	123.9	124.0	124.0
	125.1			*125.2*	*125.1*	*124.1*
N–C$_\alpha$–C$_\beta$	109.8	109.8	109.8	110.8	110.8	110.8
	110.2			*110.8*	*111.6*	*110.6*
C$_\alpha$N–NC$_\alpha$	0.2	0.2	0.0	0.2	0.2	0.0
	2.0			*0.8*	*1.3*	*31.8*

[a] Experimental data from ref 3. [b] Experimental data from ref 1. [c] Experimental data from ref 2. [d] The metal–nitrogen bond distances in the triclinic B form are distinguished with respect to the direction of stacking in the molecule. This M–N distance is parallel to the *c* axis, or stacking axis, of the porphyrin. This distinction does not apply to the triclinic A and tetragonal forms. [e] This M–N distance is normal to the stacking axis. [f] The average of all four M–N bonds.

Results from molecular mechanics calculations are listed in Table II. Specifically, the total energies and breakdowns of the energies into types for all three conformers of CuOEP and NiOEP in which the ethyl groups are oriented as found in the triclinic B, triclinic A, and tetragonal NiOEP crystals are listed. These calculations were carried out both with (italic, Table II) and without partial charges on the atoms. Addition of charge increases the total energy by ~30 kcal/mol in all cases. Regardless of the presence of electrostatic charge, however, the total energy is always slightly (~6–7 kcal/mol) higher for NiOEP than for CuOEP (see Discussion).

Table III gives a comparison of the X-ray structure (italics) and the calculated structure for some important structural parameters. For the X-ray structures, the metal–nitrogen (M–N) bond distance shown in Table III varies significantly depending on its orientation with respect to crystal packing for only the triclinic B forms of CuOEP and NiOEP. There is little variation in the skeletal bond distances either between crystals or between Ni(II) and Cu(II) derivatives. Also, the calculated and experimental values are in close agreement. The N–M–N angle (across the core of the porphyrin) and the C$_\alpha$N–NC$_\alpha$ dihedral angles show that a planar species is calculated even for the orientation of the ethyl groups observed for the ruffled tetragonal crystalline form.

Discussion

Porphyrin Stacking Geometry. More extensive π–π interactions are expected for the triclinic B phases of NiOEP and CuOEP than for the triclinic A crystals. The CuOEP triclinic A and B phases have X-ray cell parameters that are similar to those of NiOEP triclinic A and B phases[4] and are indicative of similar crystal packing. Two geometric packing parameters, the metal–metal distance (Figure 1) and the lateral shift,[21] can be directly correlated to the π–π interactions in the NiOEP and CuOEP crystals. The lateral shift is defined as the separation between the centers of

porphyrins in the crystal, measured in the direction parallel to the mean porphyrin plane. In triclinic B CuOEP, the Cu–Cu distance is 4.80 Å and the lateral shift is 3.35 Å. For triclinic A and B NiOEP, the Ni–Ni distances are 7.62 and 4.80 Å and the lateral shifts are 6.78 and 3.36 Å, respectively. For CuUroP aggregates in solution, the metal–metal distance is determined from ESR measurements to be 3.5 Å (when a lateral shift of 0 Å is assumed).[22] Large and small lateral shifts and metal–metal distances are indicative of a lesser versus a greater amount of π–π interaction between the stacked porphyrin rings. Thus, more π–π interaction is expected between rings for the triclinic B phase.

Single-Crystal Raman Spectroscopy. The extent of π–π interactions between porphyrin macrocycles in the crystalline environment can be ascertained from the degree of frequency shifts of certain Raman modes. Small but significant differences in the frequency of the oxidation-state marker lines,[6,16–18] ν_4, ν_3, ν_2, and ν_{10}, are noted (see Table I). These marker lines are sensitive to the π-charge density on the porphyrin ring, and the last three are also sensitive to core size.[5,6] The frequencies of these modes for the CuOEP triclinic B form are higher than those of the triclinic A form by 1–4 cm^{-1}, indicating that either an increase in the π–π interactions or a contraction of the porphyrin core or both are taking place. The core-size dependence of these Raman lines has recently come into question,[10] but in this case, where both triclinic A and B forms maintain porphyrin planarity, the core-size interpretation is probably valid.

The data in Table I indicate that the aggregation shifts in the Raman modes may be sensitive to a change in metal. Although the differences in the Δ(B–A) values between NiOEP and CuOEP are not statistically significant, the Δ(B–A) values for CuOEP are all slightly less than the corresponding NiOEP differences. The smaller shifts, if valid, for CuOEP are probably due to the different metal sizes. For example, the metal–metal (crystal interatomic) distances of Cu(II) and Ni(II) are 2.49 and 2.56 Å, respectively,[14] and the unconstrained equilibrium Cu–N bond (1.970 Å) is larger than the Ni–N bond (1.855 Å). All shifts upon aggregation are positive, indicating a contraction of the porphyrin core, but when the larger Cu(II) ion is present, the core does not contract as much and smaller Raman shifts are observed.

Comparison of X-ray Crystal and Calculated Structures. Except for the ethyl orientations observed in the tetragonal crystalline form (for which a planar conformation is predicted), it is apparent from Table III that there are only minor differences between the experimental and calculated structures (particularly in the angle values). The planarity of the structure with tetragonal ethyl orientations is shown in the C$_\alpha$N–NC$_\alpha$ dihedral angles, where the X-ray crystal value is 31.8° and the predicted value is 0.0°. Crystal-packing forces may be involved in allowing crystallization in the energetically unfavorable ruffled conformation. The ruffling distortion mode is "soft", requiring only small compensating energies of packing. However, the agreement for planar forms of CuOEP is roughly equivalent to that for planar forms of NiOEP, the molecule on which the force field is based.

It is apparent from comparison of bond distances and angles between the M(OEP)s with and without atomic charges that the partial charges have little or no effect on the structure, although the charges increase the total energy of the molecule. However, the differences between ethyl conformers with the same metal and the differences between corresponding conformers for different metals are significant and approximately constant. The difference in energy between the same ethyl conformers with different metals (6–7 kcal/mol) originates from two specific energy types: bond distortions and van der Waals interactions. Approximately half of the energy difference resides in the bonds and half in the van der Waals interactions. The larger energy for Ni(II) than for Cu(II) can be explained on the basis of strain in the M–N bond distances. For planar Cu– and NiOEP, the observed M–N dis-

(21) Scheidt, W. R.; Lee, Y. J. In *Struct. Bonding (Berlin)* **1987**, *64*, 1–70.

(22) Blumberg, W. E.; Peisach, J. *J. Biol. Chem.* **1965**, *240*, 870.
(23) (a) Shelnutt, J. A.; Dobry, M. M. *J. Phys. Chem.* **1983**, *87*, 3012. (b) Shelnutt, J. A. *Inorg. Chem.* **1983**, *22*, 2535. (c) Satterlee, J. D.; Shelnutt, J. A. *J. Phys. Chem.* **1984**, *88*, 5487. (d) Satterlee, J. D.; Shelnutt, J. A. *Inorg. Chim. Acta* **1985**, *106*, 165.

tances are much longer than the unconstrained bond distances. The observed M–N bond distances for CuOEP and NiOEP are 1.998 and 1.953 Å and the M–N unconstrained equilibrium bond distances are 1.970 and 1.855 Å, respectively. The differences are –0.03 and –0.10 Å for Cu- and NiOEP, indicating the greater strain in the Ni–N bond. Other skeletal bonds must also be strained to allow contraction of the metal core for NiOEP. The increase in van der Waals type energy may be explained on the basis of a slight shrinkage of the porphyrin skeleton, bringing the atoms of the porphyrin closer to the center and increasing the crowding of the peripheral substituents.

Differences in the M–N bond lengths are noted for different orientations with respect to the crystal axis for the triclinic B crystal. The length of the M–N bond in the triclinic B form is probably dictated by the presence (or absence) of π–π interactions and the ethyl substituent orientations. However, in the molecular mechanics calculations, for which an isolated M(OEP) molecule is energy minimized, the π–π interactions are not taken into account. With no interactions with other molecules, any structural differences result from the special orientation of the ethyl substituents. Similarly, observed differences in energy are due to the ethyl group orientations. On the other hand, the crystal data take into account the packing of molecules in the triclinic B crystal and hence the π–π interactions that take place within the crystal environment.

X-ray structural data on the NiOEP triclinic B crystal give Ni–N bond lengths of 1.946 and 1.958 Å.[1] The difference in length of these Ni–N bonds is statistically significant and was attributed to their orientation within the crystal with respect to the direction of stacking. The shorter Ni–N bonds are parallel and the other, longer Ni–N bonds are perpendicular to the direction of stacking. (The direction of stacking is defined to be along the stacking axis (c axis). With the consecutive four-up/four-down orientations of the ethyl substituents, a single porphyrin macrocycle can be visualized as a chair conformation. The two M–N bonds that parallel the direction of stacking of the porphyrin chairs would be along the axis of the stack.) However, for ethyls oriented as in triclinic B NiOEP, the calculated Ni–N bond distances are 1.951 and 1.954 Å, where the *longer* distance corresponds to the axis of stacking in the crystal. This calculated trend is opposite that for the Ni–N bond lengths of the NiOEP triclinic B crystal. Apparently, the π–π stacking interactions act to reverse the effect of the ethyl substituents on the M–N bonds.

For the CuOEP triclinic B crystal, the difference in lengths of the Cu–N bonds (Δ = 0.003 Å) is not statistically significant but again the shorter bond (1.996 Å) is parallel and the longer bond (1.999 Å) is perpendicular to the direction of stacking. As for NiOEP, the calculations place the shorter Cu–N bond perpendicular and the longer Cu–N bond parallel to the axis of stacking (see Table III). Thus, for both NiOEP and CuOEP the molecular mechanics calculations, which include only the effect of the ethyl group orientations and not porphyrin–porphyrin interactions due to stacking, predict the reverse M–N bond lengths. A strong π–π interaction might overcome the effect of the substituents, resulting in the significantly shortened bonds parallel to the stacking direction.

Table II shows that the calculated structure with the triclinic B ethyl orientations is the most energetically favored for both metals by ~2 kcal/mol. At still lower energy is the conformer for which the ethyl groups on each pyrrole are on opposite sides of the porphyrin macrocycle. This alternating ethyl conformer does not allow efficient packing of the OEP macrocycles however. Apparently, the most favorable tradeoff between crystal stacking and energy is therefore manifest in the triclinic B ethyl orientation. Also, it was previously noted[1] that the presence of H_2OEP promotes the formation of the triclinic A phase of NiOEP. H_2OEP is isomorphous with the triclinic A form and not the triclinic B form of NiOEP; therefore, when H_2OEP is present, NiOEP uses H_2OEP as a template for crystallization. The calculated higher energy of the triclinic A ethyl orientations may be why the presence of the H_2OEP template is required.

Comparison of Crystalline and Solution Raman Data. The

metallouroporphyrins provide a novel means of investigating aggregation phenomena in solution.[8,19,22,23] The uroporphyrins are monomeric in aqueous base below 1×10^{-3} M because of the electrostatic repulsion resulting from their high peripheral charge (–8). Under acid or high ionic strength (>1 M) conditions the charge is shielded and they aggregate or dimerize. For example, CuUroP at 1×10^{-4} M dimerizes at 5.5 M salt concentration as evidenced by a 16-nm blue shift in the Soret band and 3-nm red shift in the α band.[19] In NiUroP a 13-nm blue shift of the Soret band and a 3-nm red shift in the α band was observed.[19]

In contrast with the large effect of dimerization on the absorption spectrum, only small shifts are found in the Raman marker lines. Nevertheless, the Raman results for the triclinic crystals mimic well the results from solution studies of CuUroP π–π aggregation. For example, the aggregation-induced shifts in ν_4, ν_3, ν_2, and ν_{10} for CuUroP are 1.3, 2.6, 0.7, and 2.7 cm^{-1} and are similar to differences of 1.0, 3.9, 2.6, and 2.4 cm^{-1} for the CuOEP triclinic forms (Δ(B–A) in Table I). Thus, aggregation in the crystal causes shifts in the core-size markers similar in magnitude (1–4 cm^{-1}) and direction (an increase) to those for the solution aggregates. The same general pattern of marker line shifts is observed upon formation of Ni-, Fe(OH)-, Pt-, and PdUroP salt dimers.[1,19]

Table I shows that Δ(B–A) for ν_2 of CuUroP is unusually low (0.7) compared to that for the M(OEP)s (-2.8). This low value may be due to the orientation of the ethyl substituents in solution. Instead of the chair ethyl orientations of the triclinic B crystal, CuUroP dimers probably have all eight carboxylate substituents oriented on the same side of the macrocycle and pointing away from the other macrocycle of the dimer. This orientation is preferred because of the repulsion of the negatively charged carboxylates of the propionate and acetate side groups of uroporphyrin and may be the cause of a low Δ(B–A) value for ν_2 of CuUroP. Unlike the other core-size-sensitive Raman lines, ν_2 primarily consists of the porphyrin C_β–C_β stretching vibration,[11] and the C_β's are the point of attachment for the eight propionate and acetate substituents in the UroPs. Significant change in ν_2 between the OEPs and the UroPs may be expected because of the differing substituent orientations. However, the Δ(B–A) value for ν_2 of NiUroP is more comparable to those of NiOEP and CuOEP than to that of CuUroP.

Conclusions

Differences in the Raman spectra of CuOEP triclinic A and B phases can be interpreted in terms of π–π interactions found only in the triclinic B phase. The Raman results suggest that π–π interactions in the crystalline triclinic B phase cause a decrease in π-charge density in the porphyrin ring. The decrease in π charge causes a contraction of the porphyrin core. On the basis of the frequency differences observed for "dimer" (B form) and "monomer" (A form) crystal packing and the increase in frequency for the core-size marker lines, ν_3, ν_2, and ν_{10} (assuming 0.0022, 0.0026, 0.0019 Å contraction per wavenumber increase),[6] we expect a slight contraction of the porphyrin core of between 0.005 and 0.009 Å.

Core contraction was observed in a comparison of the triclinic X-ray structures, where a contraction of 0.006 Å in the average Ni–N bond distance in the triclinic B compared to the triclinic A form was reported.[1] Although there is no X-ray crystal structure for triclinic A CuOEP, it has been shown[4] that the crystal packing must be similar to that in triclinic A NiOEP. We thus predict a larger core for the CuOEP triclinic A form than for the triclinic B form on the basis of the Raman marker line frequencies.

The bond distances and bond angles obtained from molecular mechanics calculations agree with X-ray crystal structures with the exception of the ethyl orientations for tetragonal NiOEP, for which a planar conformation is predicted. However, the calculations reverse the trend of M–N bond length with respect to the stacking axis, most likely because no porphyrin–porphyrin interactions are considered. Also, the addition of electrostatic charge has little effect on M(OEP) porphyrin structure. The structure with the triclinic B ethyl orientations was shown to be the most

energetically favored conformation of all the ethyl conformers observed in the crystals.

Another important result of the Raman investigation is that π–π aggregation in the triclinic B crystals of both Cu- and NiOEP results in structural changes similar to those occurring upon aggregation in solution. This similarity is observed in spite of probable differences in substituent orientations in the solution and crystal cases. This result indicates that it is the π–π interactions that are important in determining the monomer–aggregate

structural differences, not the substituent orientations.

Contribution from the Debye Research Institute, University of Utrecht, The Netherlands

Luminescence of Copper(I) Arenethiolates and Its Relation to Copper(I) Luminescence in Other Complexes

D. Martin Knotter,[1a] George Blasse,*[1b] Jacques P. M. van Vliet,[1b] and Gerard van Koten*[1a]

The luminescence properties of some trinuclear copper(I) arenethiolates are reported and discussed. Two of these copper(I) arenethiolates, i.e., [CuSC$_6$H$_4$[(R)-CH(Me)NMe$_2$]-2]$_3$ and [Cu$_3${SC$_6$H$_4$[(R)-CH(Me)NMe$_2$]-2}$_2$(C≡Ct-Bu)]$_2$, show triboluminescence. The optical transitions in these copper(I) compounds are assigned to ligand-to-metal charge transfer (LMCT). It is proposed that the formation of a three-electron two-center sulfur–sulfur bond in the excited state lowers the excitation energy of these trinuclear copper(I) arenethiolates. Structural information about lone pair orientation in copper(I) arenethiolates can be derived from UV/vis data as is shown for [CuSC$_6$H$_4$(CH$_2$NMe$_2$)-2]$_3$. A comparison with optical transitions on Cu(I) complexes reported in the literature is also made.

Introduction

It is well known that certain Cu(I) complexes show efficient luminescence.[2,3] The nature of the transition involved has been interpreted in different ways. On the one hand, the transition has been ascribed to a metal-to-ligand-charge transfer (MLCT) where an electron is transferred from the copper(I) center to the unoccupied π^* orbital of the ligand.[3] On the other hand, the occurrence of a metal-centered transition is also possible. In this case an electron is promoted from the 3d level to the 4s or 4p level.[4]

Recently we reported the synthesis and structural characterization of a novel class of copper(I) arenethiolates, [CuSC$_6$H$_4$-[(R)-CH(Me)NMe$_2$]-2]$_3$ (1; [CuSAr']$_3$) and [CuSC$_6$H$_4$-(CH$_2$NMe$_2$)-2]$_3$ (2; [CuSAr]$_3$).[5] These compounds have a trinuclear structure, and 1 has been structurally characterized (shown in Figure 1a) by a single-crystal X-ray structure determination. Particular interesting features of these compounds are the chair-like conformation of the six-membered Cu$_3$S$_3$ ring, the equatorial binding of the aryl groups to the Cu$_3$S$_3$ ring, and the intramolecular coordination of each of the *ortho*-CH(Me)NMe$_2$ substituents to a copper atom, resulting in a trigonal coordination geometry of each of these atoms (see Figure 2a). Strong evidence for a second possible structure for these compounds has been obtained from NMR studies in which one of the three aryl groups is axially bonded to the Cu$_3$S$_3$ ring (see Figure 2b).

Replacement of one of the arenethiolate groups by an alkynyl group (C≡Ct-Bu) resulted in the synthesis of a further class of novel copper(I) arenethiolates, [Cu$_3$(SAr')$_2$(C≡Ct-Bu)]$_2$ (3) and [Cu$_3$(SAr)$_2$(C≡Ct-Bu)]$_2$ (4), which have the hexanuclear

structure shown in Figure 1, parts b and c, respectively.[6] These structures are brought about by dimerization of two trinuclear units [compare the schematic structures of [CuSAr]$_3$, a and b, with the Cu$_3$(SAr)$_2$(C≡Ct-Bu) units, c and d, of [Cu$_3$(SAr)$_2$-(C≡Ct-Bu)]$_2$ in Figure 2]. These monomeric units consist of a six-membered Cu$_3$S$_2$C ring in the boat conformation, with the aryl groups bonded either one equatorially and one axially (Figure 2d) or exclusively axially (Figure 2c) to the Cu$_3$S$_2$C ring.

A remarkable feature of these compounds is that the chiral compounds 1 and 3 show an intense triboluminescence which is visible even at broad daylight. Upon mechanical disruption the crystals emit light. This prompted us to study the photoluminescence properties of this type of compounds in more detail. We have studied the latter, because the triboluminescence is difficult to measure and the triboluminescence spectra are usually comparable to the photoluminescence spectra.[7,8] This was by visual inspection also the case for the present compounds.

Experimental Section

(1) (a) Laboratory of Organic Chemistry, Department of Metal-Mediated Synthesis, Padualaan 8, 3584 CH Utrecht, The Netherlands. (b) Physics Laboratory, P.O. Box 80000, 3508 TA Utrecht, The Netherlands.
(2) Eitel, E.; Oelkrug, D.; Hiller, W.; Strähle, J. *Z. Naturforsch.* **1980**, *35b*, 1247.
(3) Blasse, G.; McMillin, D. R. *Chem. Phys. Lett.* **1980**, *70*, 1.
(4) (a) Pedrini, C. *Phys. Status Solidi B* **1978**, *87*, 273. (b) Chermette, H.; Pedrini, C. *J. Chem. Phys.* **1981**, *75*, 1869.
(5) (a) Knotter, D. M.; van Koten, G.; van Maanen, H. L.; Grove, D. M.; Spek, A. L. *Angew. Chem.* **1989**, *101*, 351. (b) Knotter, D. M.; van Maanen, H. L.; Grove, D. M.; Spek, A. L.; van Koten, G. *Inorg. Chem.* **1991**, *30*, 3309.

(6) (a) Knotter, D. M.; Spek, A. L.; van Koten, G. *J. Chem. Soc., Chem. Commun.* **1989**, 1738. (b) Knotter, D. M.; Spek, A. L.; Grove, D. M.; van Koten, G. *Organometallics*, submitted.
(7) (a) Zink, J. I. *Acc. Chem. Res.* **1978**, *11*, 298. (b) Zink, J. I. *Naturwissenschaften* **1981**, *68*, 507.
(8) Chandra, B. P.; Zink, J. I. *Phys. Rev. B* **1980**, *21*, 816.
(9) van Vliet, J. P. M.; Blasse, G.; Brixner, L. H. *J. Electrochem. Soc.* **1988**, *135*, 1574.